analytical chemistry

pubs.acs.org/ac Article

Automated Programmable Generation of Broad pH Range Volatile Ionic Eluents for Liquid Chromatography

Charles Phillip Shelor,* Kenji Yoshikawa, and Purnendu K. Dasgupta*

Cite This: *Anal. Chem.* 2021, 93, 5442−5450 Read Online

ACCESS | Metrics & More | Article Recommendations | Supporting Information

ABSTRACT: Many of the universal detectors in liquid chromatography, including mass spectrometry, must completely volatilize the chromatographic eluent first before further processing and detection of the analytes. A basic requirement is that the eluent does not contain a nonvolatile dissolved component. However, separation of biomolecules must be conducted in mostly aqueous media of compatible pH and ionic strength if their biological activity must survive the separation process. Combinations of ammonia with acetic and formic acids are commonly used as eluent for this purpose but generally maximum concentrations that can be tolerated are relatively low. Further, buffering is good only over a limited pH range. We describe a system where the eluent is generated in an automated pressure-programmed manner from high-purity gaseous NH_3 and CO_2 through gas-permeable membrane devices. This can be aided by the prior presence of formic/acetic acids in the mobile phase to extend the attainable low pH limit. We outline the fundamental pH, ionic strength, and buffer intensity considerations and demonstrate the application of such eluents in the separation of amino acids, proteins, and monoclonal antibodies. We also demonstrate the use of dissolved CO_2 as an ion-pairing agent in the separation of chiral amines.

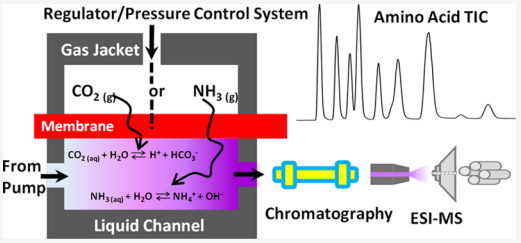

INTRODUCTION

Aside from convenience, automation eliminates human error and reduces contamination, improving reproducibility. Ion chromatography (IC) is unique among chromatographic techniques to provide automated current programmed eluent generation. Introduced in 1991,[1] this principle has enjoyed considerable commercial success. A variety of electrodialytic generators in different scales and those capable of generating buffers with linear gradients in pH and ionic strength have since been described (see ref 2 for a recent example and ref 3 for a recent review). Also beginning in 1991, Olesik et al. introduced enhanced fluidity liquid chromatography (EFLC) in which liquid CO_2 was mixed with polar organic mobile phases to address poor solvent polarity of CO_2 as used in supercritical fluid chromatography (SFC).[4] This approach has matured; current systems permit ternary gradients[5] and can perform challenging bioseparations, aided by tandem mass spectrometry (MS/MS).[6] Preparative scale use is being explored.[7] The solubility of CO_2 in methanol is much higher than that in water (at 25 °C Henry's law constants in methanol range from 0.178 to 0.234 m/atm[8,9] compared to 0.031−0.045 m/atm in water[10]). Solubility increase due to the ionization of H_2CO_3* (the sum of $CO_2{\cdot}H_2O$ and true H_2CO_3[11]) is very small. Methyl hydrogen carbonate is also similarly formed in a methanol−CO_2 mixture,[12] albeit this formation is also likely small.

Rather than introducing liquid CO_2 SFC-style, CO_2 has been introduced recently into flowing aqueous streams through a gas-permeable membrane (GPM) to make CO_3^{2-}/HCO_3^- based eluents for IC[13] or H_2CO_3* for ion exclusion chromatography of organic acids.[14] With a novel frit-supported silicone membrane engasser that permits CO_2 pressures up to ~900 psi, ≥0.5 M [H_2CO_3*] is possible. This has been used for both gradient and isocratic elution of cations.[15] Multiple patents exist on frit-supported membranes to carry out engassing/degassing into/from liquids at high pressures.[16,17] The vast differences in solubility of CO_2 in methanol vs water, and the pressures involved ensure vastly different eluent CO_2 contents in these approaches vs those in EFLC. Certainly, these eluents display no enhanced fluidity, but they are green in being purely aqueous.

Increasingly, the best complement to high-performance liquid chromatography (HPLC) is mass spectrometry (MS) detection, the most common interface being electrospray ionization (ESI). Nonvolatile residues on the ion source must be avoided. Similar requirements exist for the use of other universal detectors like the charged aerosol detector[18] (CAD, widely used in the pharmaceutical industry[19]), the evaporative light scattering detector,[20] and other aerosol-based detectors.[21] However, best separations are often obtained at significant

Received: December 4, 2020
Accepted: March 15, 2021
Published: March 24, 2021

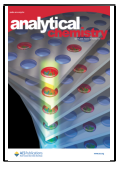

https://doi.org/10.1021/acs.analchem.0c05089
Anal. Chem. 2021, 93, 5442−5450

salinities using pH and ionic strength gradients, typically incompatible with the above detectors.

The same considerations apply to ion-pair chromatography (IPC); many of the traditional IP agents were nonvolatile. During the early stages of liquid chromatography-electrospray ionization-mass spectrometry (LC-ESI-MS), the use of various amines[22] and low-MW alkanoic/perfluroalkanoic acids[23] were advocated as volatile IP agents for the analysis of acidic and basic analytes, respectively. However, these were often not optimal, a recent paper provides statistics on the dramatic decrease of the use of IPC over the intervening period.[24]

For mostly aqueous eluents used in LC-ESI-MS, which are usually based on ammonium acetate or formate, the maximum recommended concentration is <25 mM, preferably <10 mM with an eluent pH within 2 units of analyte pK_a,[25] with the vast majority of reported applications using ≤10 mM salt;[26] albeit higher salt concentrations are possible under high organic content EFLC conditions[27] or in nanospray MS applications.[28] Higher salt concentrations may be possible under other conditions, but significant ionization suppression occurs, especially with purely aqueous eluents.

We have the following objectives in the present paper, all demonstrated for the first time: (a) automated programmable generation of an ionic aqueous eluent from high-purity cylinder gases; (b) exploit the complete volatility of this eluent in showing its compatibility with detectors that require this, particularly with an MS, (c) the successful use of carbonic acid as an IP agent, and (d) provide the theoretical framework and detailed properties of an aqueous NH_3−CO_2 buffer system as generated from the gaseous precursors.

PRINCIPLES

Equilibrium Considerations. Most of our experiments were conducted with purely aqueous eluents. As such, well-known equilibrium constants applicable to NH_3 and CO_2 and hydrolytic products derived therefrom apply. The relevant equilibrium constants presently used in the numerical simulations below are listed in the Supporting Information (SI). The NH_3−CO_2 system is compared with the NH_3−NH_4OAc/NH_4OHCO−AcOH/HCOOH systems. None of the computations accounted for activity corrections. Rather than imagining a solution simultaneously in equilibrium with a given pCO_2 and pNH_3, much like our experimental arrangement, we model a stream of pure water equilibrated with a given pCO_2 being mixed with another stream equilibrated with a given pNH_3. We assume complete gas−liquid equilibration in each stream with a pCO_2 range of 0−10 atm, a pNH_3 range of 0−0.04 atm, and a 3:1 flow ratio. The differences in the ranges and the flow rates reflect the >1500× differences in the intrinsic solubility of the two gases and the stronger basicity of NH_3 compared to the acidity of H_2CO_3*. It is important to note that complete gas−liquid equilibration represents the theoretical limit; this is only approached when the engasser residence times are sufficiently long. The reader would appreciate that all of the computed properties depend ultimately on the pCO_2 and pNH_3 levels in the respective equilibrated aqueous streams. Whether these are reached by a combination of high gas pressures and a relatively low attainment of equilibrium or low gas pressures and a much closer approach to equilibrium is not important. For ammonia, if one operated under conditions of a higher degree of equilibration in the engasser, a diluted gas standard, e.g., 1−10% NH_3 in N_2, and/or mass flow controlled deliveries would be preferred because the necessary pNH_3 levels are so low.

Table S1 in the SI presents the entirety of the computed results as any reasonable number of graphical representations will not capture the entire horizon. Figure 1 shows the pH surface obtained from variations in pCO_2 and pNH_3 in the range indicated, see Figure S1 for a contour plot. Vertical slices of Figure 1 topographic surface are each essentially a titration curve, starting with NH_3 and adding CO_2. While the minimum to maximum pH values range from 3.4 to 11.5, these extremes correspond to CO_2 only and NH_3 only and have essentially no buffering ability, particularly at the low pH end. This is more clearly seen in the two-dimensional (2D) buffer intensity vs pH plot (Figure 2) (see Figure S2 for a three-dimensional (3D) rendition). The system can attain >10 mM/pH unit buffer intensity in the pH range 4.5−10.75. The two peak buffering regions correspond to the pK_a of HCO_3^- (6.4) and NH_4^+ (9.25), the location (pH 9.28), and the magnitude of the second maximum are influenced by additional buffering from

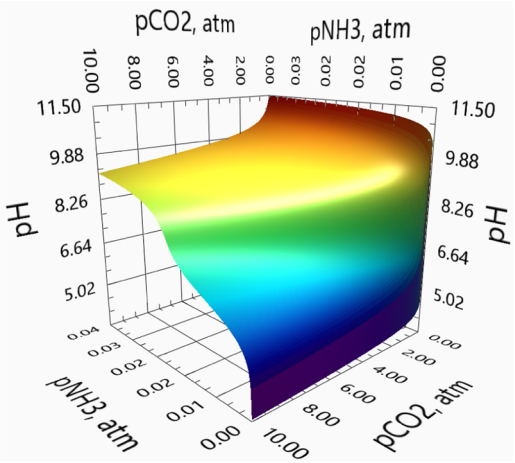

Figure 1. Three-dimensional representation of the pH surface obtained from variations in the pCO_2−pNH_3 equilibrium system with mixing of the respective individual solutions in a 3:1 volume ratio.

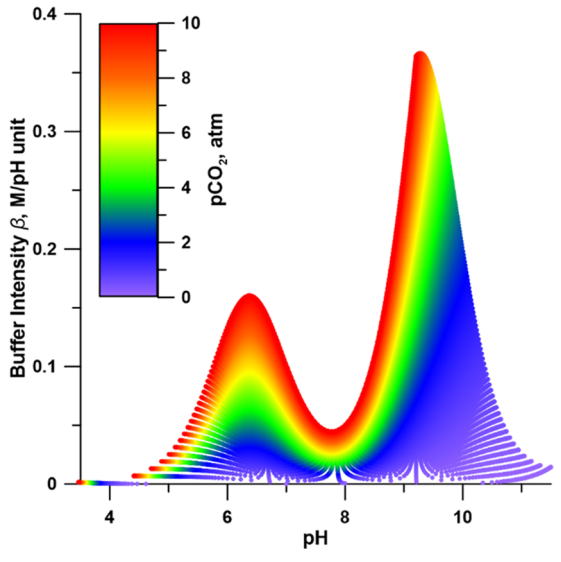

Figure 2. Buffer intensity in the system of Figure 1.

https://doi.org/10.1021/acs.analchem.0c05089
Anal. Chem. 2021, 93, 5442−5450

the HCO_3^-–CO_3^{2-} system. The buffering capacity enters a valley region around pH 7.8 but even here, a β value >45 mM/pH can be readily attained (see Figure S2). In this context, note that except at the very low pH end, the change in pH in any vertical slice of the pH surface in Figure 1 is gradual, indicating good buffering. While the high end of the attainable pH is adequate for most separations, extending improving buffering at the low pH end will be desirable.

The solid lines in Figure 3 represent a gradient being run between 20 mM HCOOH and 20 mM NH_4OH (solvents A and B). At these concentrations, the NH_4OHCO salt concentration remains ≤10 mM, as recommended to avoid ion suppression. The pH profile vs %B is the expected titration curve, with a relatively sharp pH transition near the equivalence point, where β essentially goes to zero. At the present concentrations, there is little buffer capacity in this system, <5 mM/pH unit, in the important intermediate pH range of 4.2–8.8; see also Figures S3 and S4 in the SI for further depictions of this system and Figures S5 and S6 for the corresponding NH_4OAc system, which differ essentially only in being shifted 1 pH unit higher than the NH_4OHCO system. Adding a further 10 mM NH_4OHCO does not much improve β at intermediate pH values.

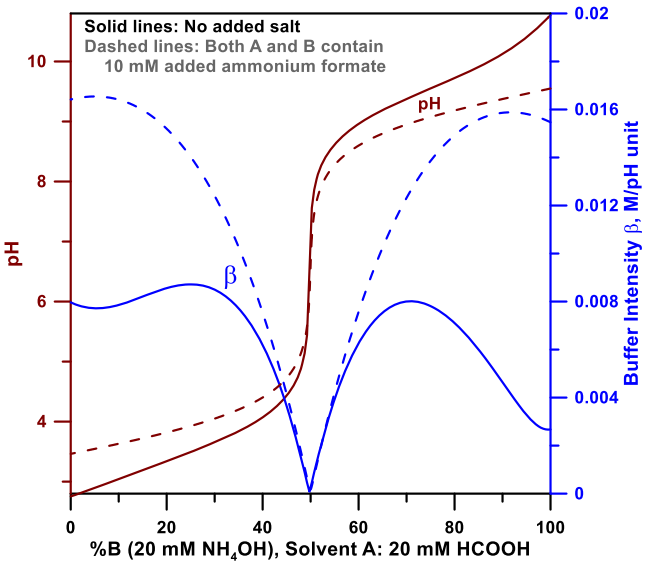

Figure 3. pH and buffer intensity with a linear gradient run between HCOOH (pK_a 3.74) and NH_4OH, each 0.02 M (solid lines); additional 0.01 M NH_4OHCO present (dashed lines).

With NH_3–HCOOH/CH_3COOH systems, an extended pH range eluent with appreciable buffer capacity throughout is obviously not possible. In contrast, the broad pH range buffering ability of NH_4HCO_3 has been noted by others as well.[29] The deficiency in β at the low pH end in this system (Figure 2) can be solved by adding a modest amount of HCOOH. Even without the addition of any salt-forming base, HCOOH is sufficiently ionized (pK_a 3.74) to provide an appreciable buffer capacity (Figure 3).

EXPERIMENTAL SECTION

The general experimental arrangement is shown in Figure 4. Two different types of engassers have been previously described and used with CO_2.[13,14] Although chemically inert, dissolution of gases in the polymer can make Teflon AF (TAF) brittle and limit usable pressures. However, TAF capillary engassers, 0.18/0.68–0.74 mm i.d./o.d., with thick-walled 3 mm i.d. tubular poly(tetrafluoroethylene) (PTFE) jackets, safely permit pCO_2 and pNH_3 up to at least 15 atm. They were used in this work to introduce each gas individually. In each case, the gas of interest is introduced into the engasser through a normally closed ethylene propylene diene monomer (EPDM) elastomer stainless steel solenoid valve (52G8DKM-AB, www.peterpaul.com; Viton seals are incompatible with NH_3). The engasser jacket is vented via another similar valve. Gas pressures are monitored on either inlet or outlet side of the engasser jacket using 250 psig pressure transducers (P/N 40PC250G2A, 5 V FS, www.honeywell.com) off tees.

Figure S7 includes details not shown in Figure 4 for clarity, e.g., capillary restrictors (20 cm long 150 μm i.d. fused silica capillaries) at the inlet/outlet of each engasser to avoid pressure shocks. With ammonia, adiabatic expansion leads to significant cooling. Despite the low water permeability of TAF,

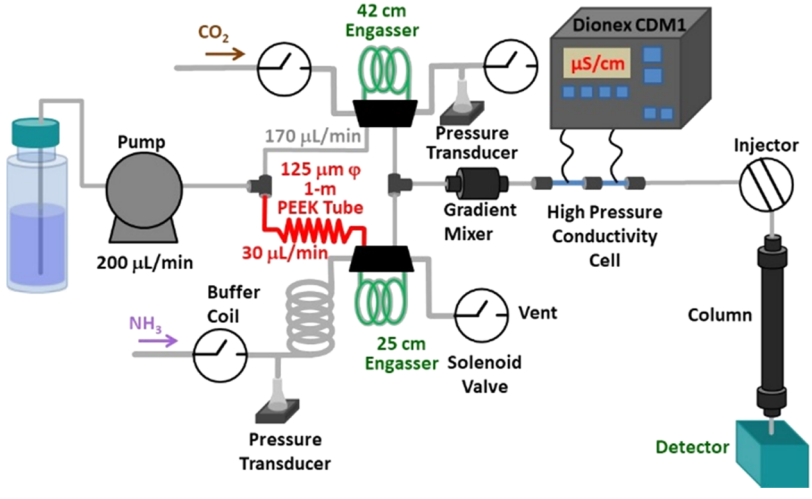

Figure 4. Experimental system, general schematic. The pumped stream (water or dilute HCOOH) is split into two, the major and minor (typ. 3:1) flows proceed, respectively, through CO_2 and NH_3 engassers and are then recombined at a gradient mixer prior to proceeding to a high-pressure conductivity cell, injector, column, and detector.

https://doi.org/10.1021/acs.analchem.0c05089
Anal. Chem. 2021, 93, 5442–5450

the water flowing through the TAF capillary is under high pressure. Sufficient water vapor can permeate out and condense at a lower temperature. This traps ammonia by dissolution, making a reservoir. A buffer/delay coil (ca. 2 m, 1.6 mm i.d.; ∼4 mL of volume) was therefore provided between the ammonia introduction capillary and the engasser entrance. For the same reason, a buffer/delay coil (ca. 2 m, 1.6 mm i.d.; of ∼4 mL volume) was provided between the ammonia introduction capillary exit and the engasser entrance. A heating tape is provided around the restrictor and the buffer coil to prevent condensation. The engasser also needs venting to return to zero pressure. Venting small amounts of CO_2 to the ambient air does not pose a hazard; we have occasionally used a soda-lime trap. Ammonia can be odorous at low levels, however, and toxic at higher levels; it must be vented through an acidic trap. We have used sulfuric acid impregnated silica gel.[30] A liquid acid trap is not recommended: the vacuum created by NH_3 dissolution may lead to aspiration. Note that venting to atmospheric pressure still allows 1 atm absolute pressure of the gas to be present in the enclosure. For a high-permeability high-solubility gas like NH_3, this will lead to an undesired level of uncontrolled NH_3 introduction; unacceptable especially when a low eluent pH is desired. When no NH_3 introduction is desired, e.g., when beginning a low to high pH-gradient run, any residual NH_3 in the engasser can be swept out by N_2 introduced through a tee and an additional solenoid valve. Alternatively, a three-way valve with a vacuum source is placed after the acid trap. This allows the engasser jacket to be either just vented or subjected to vacuum (Figure S7). The extent of the residual NH_3 issue is greatly ameliorated if a diluted NH_3 standard, rather than pure NH_3, is used.

As to CO_2, hydration is slow and if pure H_2CO_3* is to be used as eluent, a hydration coil is essential to provide some reaction time after the CO_2 engasser.[14,15] Presently, the immediate contact of the carbonated stream with an alkaline solution rapidly produces HCO_3^-; a hydration coil was not needed.

Engasser Control and Calibration. Both engassers were operated under nonequilibrium (kinetically controlled) conditions; permeation rates were experimentally determined. Two stainless steel tubes joined by a nonconductive union forms the high-pressure conductivity cell (Figure 4) monitored by a CDM-I conductivity detector (www.dionex.com). This detector serves multiple functions, including the calibration of gas introduction rates. Details for calibrating a CO_2 engasser were previously given.[13] Briefly, a standard solution of an alkali hydroxide (often electrodialytically generated) is pumped through the CO_2 engasser and the conductivity is continuously monitored downstream as pCO_2 is slowly increased. Starting from the high conductance of an alkali hydroxide, the conductance decreases in two stages, as OH^- is converted to CO_3^{2-} and then as CO_3^{2-} is converted to HCO_3^-. The engasser can also be calibrated directly from the conductivity of the CO_2 solution introduced into pure water. In this case, the CO_2 solution must first reach hydration equilibrium. From the known overall conductance, and the equivalent conductance values of H^+ and HCO_3^- (present obligatorily in equal concentrations from the dissociation of H_2CO_3), the concentration of each ion can be computed. Through the known dissociation constant, [H_2CO_3*] may then be calculated. A similar nontitrimetric/direct conductometric approach is easier to practice for NH_3, as hydration equilibrium is instantaneous. The introduced NH_3 stream may also be calibrated by conductometric flow titration with a known concentration of a standard acid solution. Thus, TAF ammonia engassers (5.5−160 cm) were calibrated by direct conductometry or by flow titration with HNO_3 (prestandardized with Na_2CO_3). Calibrated NH_3 streams were then used to calibrate CO_2 streams by conductometric titrations, either at constant pNH_3 and varying pCO_2 or vice versa. Faster dissolution, greater dissociation, and higher solubility all lead to less flow rate dependence in direct conductometric NH_3 calibrations, compared to that for CO_2. Engasser pressure control/relevant data acquisition was performed with a programmable system on a chip (PSoC5LP, www.cypress.com, Figure S7).

Chromatographic Equipment and Detectors. A TSQ Quantum Discovery Max Triple Quadrupole MS, with a heated electrospray source, was used for MS detection, along with a IS25 isocratic pump, and a LC30 column oven. The charged aerosol detector was a Corona Veo RS (evaporator temp: 50 °C), and the optical absorbance detector was a PDA-100; these were used with a GP40 gradient pump; Chromeleon was used for data acquisition and system control (all above were from Thermo Fisher Scientific). Injection volume was 10 μL throughout except as stated.

RESULTS AND DISCUSSION

Engassers and Introduction Rates. Engassers comprise pressurized gas on one side of a membrane and a flowing receptor liquid on the other. Aside from the capillary engassers used here, frit-supported membrane engassers use a flow-through channel between two membranes supported on rigid metal frits, while pressurized gas is present on the other side of each frit.[15] This latter design permits much higher operating pressures as well as thinner membranes and in principle permits different gases to be introduced through each side. The capillary engassers were adequate for the present purpose. However, much higher pressures are not possible in the present format, especially for NH_3. The process of gas permeation involves dissolution in the membrane and diffusion across it. As previously noted, a high degree of dissolution of the gas may catastrophically alter the bulk properties of the membrane. During early efforts to make an electrodialytic hydroxide eluent generator,[1] experiments with a stainless steel frit backed up Pd membrane as cathode failed because hydrogen loading of Pd caused a dramatic increase of the resistance of Pd.[31] As ammonia dissolves in TAF, it embrittles the polymer. TAF capillaries permit $pNH_3 \leq 10$ atm.

Illustrative direct conductometric measurement of ammonia permeation rate is shown in Figure S8, while conductometric titration to determine CO_2 is shown in Figure S9. The 42 cm CO_2 and 25 cm NH_3 engassers used in this work were found to introduce the respective gases at rates of 4.26 ± 0.07 and 3.41 ± 0.02 μmol/min/atm. When expressed per unit length, NH_3 engassers in lengths of 5.5, 25, 40, and 160 cm exhibited permeation rates of 146 ± 0, 136 ± 1, 133 ± 7, and 122 ± 4 nmol/min/cm/atm. The rate per unit length decreases with increasing length as a buildup of ammonia in the lumen reduces the effective gradient. The permeation rate per unit length is expected to decrease in an exponential fashion with the engasser length. This is observed (Figure S10), with a no-buildup limiting rate being predicted as 159 nmol/min/cm/atm.

The conductivity of the prepared eluent is one bulk property that can be monitored at chromatographic pressures without

https://doi.org/10.1021/acs.analchem.0c05089
Anal. Chem. 2021, 93, 5442−5450

difficulty. In Table S1, we estimate the conductivity of the solution. Figure S11 shows that these are linearly related to the ionic strength I regardless of pH. However, infinite dilution equivalent conductance data (λ^0) are used in the calculations, making the estimates higher than real values. Actual λ values will be increasingly lower at concentrations >10 mM. While a linear relationship between the actual conductance and I is therefore not expected, the actual conductivity will still be a monotonic function of I. The concentrations are in the range where the conductance is expected to be proportional to $\sqrt{I}$.

Carbonic Acid as an Ion-Pairing Agent. While carboxylic acids and their perfluorinated counterparts have been extensively used as negatively charged ion-pairing agents, we know of no reports on the use of carbonic acid for the purpose. For preparative separations of bases such as chiral amines, important drug precursors, this can be potentially useful. An isopropyl derivatized cyclofructan bonded stationary phase (LARIHC CF6-P, www.azypusa.com) was found particularly useful for the enantiomeric separation of a variety of primary amines.[32] The recommended conditions for the separation of racemic 1-(1-naphthyl)ethylamine involve the normal phase mode, using a heptane/ethanol eluent containing trifluoroacetic acid and triethylamine (TEA). The TEA serves to block the exposed silanol sites on the column. Baseline separation (R_s 1.7) was possible on a 25 cm column with an average N of 14 400/m. Considering potentially greater solubility of CO_2, we chose a polar organic eluent alternative, comprising acetonitrile−methanol, also possible with this column. Figure 5 shows the separation of 1-(1-naphthyl)-

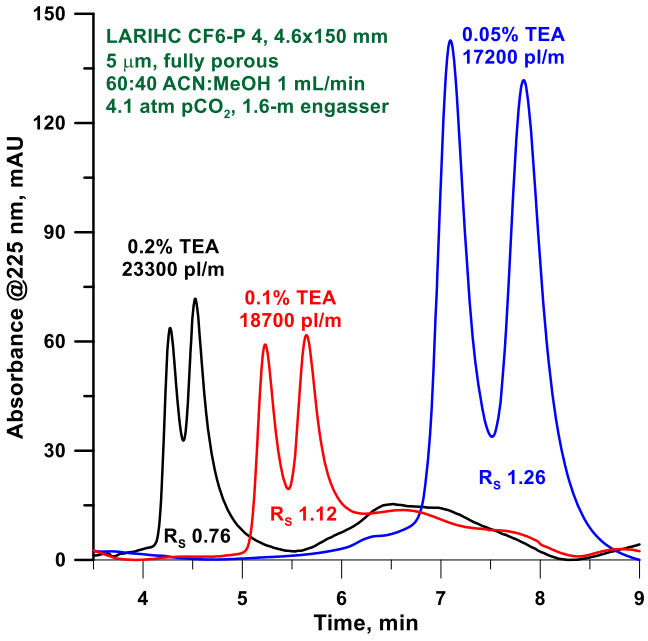

Figure 5. Chiral separation of 50 mg/L 1-(1-naphthyl)ethylamine on an alkyl derivatized cyclofructan column. See also Figure S12 for a discussion of lack of peak area conservation.

ethylamine at three different TEA levels on a 150 mm column. Although efficiency decreases with the decreasing TEA level, retention, selectivity, and resolution increase. Although neither the CO_2 nor the TEA concentrations have been optimized, at 0.05% TEA, the efficiency was better than that reported for a normal phase eluent.[32] Resolution on a 250 mm column is projected to be essentially the same as that reported for that benchmark. Figure S12 shows that both TEA and CO_2 are necessary for the analyte to elute. However, even when both are present, no chiral selectivity is observed in the presence of water. Other chiral separations on this column using 0.05% TEA and the same level of CO_2 in 60:40 ACN/MeOH are illustrated in Figure S13.

Separation and Measurement of Amino Acids. An amino acid analyzer was the first liquid chromatograph;[33] some more than six decades after the original Nobel-winning work, some commercial amino acid analyzers[34] utilize an identical process of cation-exchange separation using multiple buffers, postcolumn chromogenic reaction with ninhydrin, and dual wavelength absorbance detection. Another leading vendor uses the anion-exchange mode with a high capacity column (60 μeq for a 2 × 250 mm column) and pulsed amperometric detection with catalytic oxidation on a gold electrode. The eluent is maintained at a very high pH (≥12.6) throughout to keep even the most basic amino acids in the anionic form. Eluting power is provided by high concentrations of hydroxide and in the later parts of the gradient, acetate. Such a high eluent pH is not possible with just ammonia. Low hydroxide concentrations can not only keep basic amino acids in the anion form, it also provides poor eluting power. Added CO_2 can make carbonate, a powerful eluent, but pH decreases, making it difficult to govern retention in a controlled fashion. MS detection does not require complete physical separation of all analytes. Figure S14 shows the best-case separation we observed with MS detection on this anion-exchange phase with a NH_3−CO_2 eluent. While MS detection was successful in the presence of large amounts of NH_3 and CO_2, the separation left a lot to be desired.

In the cation-exchange mode, the problem may be opposite. Without a low enough pH, low pI analytes, e.g., aspartic acid, will be anionic and not be retained. It is easier to incorporate HCOOH in the eluent to get to such a pH than rely on CO_2 alone. It is possible to introduce AcOH or HCOOH permeatively through the same tubular engassers using temperature/pressure for control. Demonstrative data are shown in the SI (Figures S15−S18). However, below we have simply used dilute HCOOH or AcOH as the engasser influent. Separations on strong acid type cation exchangers appear in Figures 6 and 7, respectively using a low-capacity column (CG3 + CS3, courtesy Dionex.com, 36 μeq in 4 × 50 mm + 4 × 250 mm guard + separator, 10 μm) and a short efficient column (2622SC type PH, 6 × 40 mm, 3 μm, courtesy Hitachi-hta.com, exact capacity is proprietary according to the vendor). The Hitachi column (Figure 7) is available in two versions, one meant for protein hydrolysate (PH) samples and the other for physiological fluids (PF). Several amino acid separations on the PF column are shown in Figures S20−S24; vendor-recommended separations on these columns use step gradients five different eluents and eight or more temperature steps.[35] In all separations on strong cation-exchange columns, the eluent AcOH/HCOOH plays a role only in the beginning, to keep the eluent pH sufficiently acidic to retain the most acidic amino acids. Once neutralized to form NH_4^+, NH_4^+ becomes the effective eluent ion. As long as enough CO_2 is added to supply HCO_3^- as the counterion, the presence of AcOH/HCOOH in the eluent is not needed at pH ≥ 4.

In Figure 6, note the addition of a small initial NH_3 pulse; this converts some portion of the column to NH_4^+ in a controlled fashion. This functions to temporarily reduce the effective column capacity. The $[H^+]$ provided by 20−60 mM

https://doi.org/10.1021/acs.analchem.0c05089
Anal. Chem. 2021, 93, 5442−5450

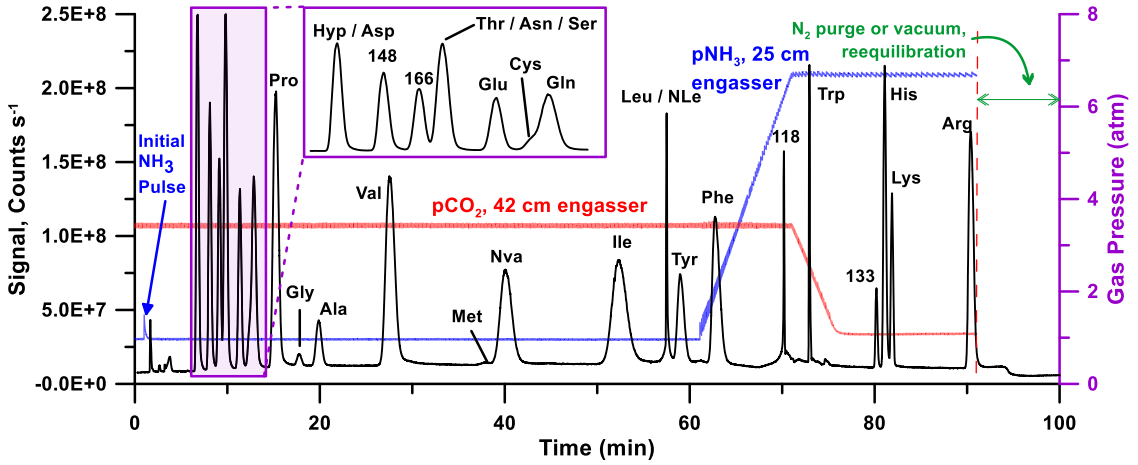

Figure 6. Separation of 23 amino acids (0.1 mM each) on a CG3−CS3 4 mm cation-exchange column set. The engasser influent is 20 mM HCOOH@1 mL/min, 30 °C. Figure S19 shows more details, peak identification, and the relevant extracted ion chromatograms.

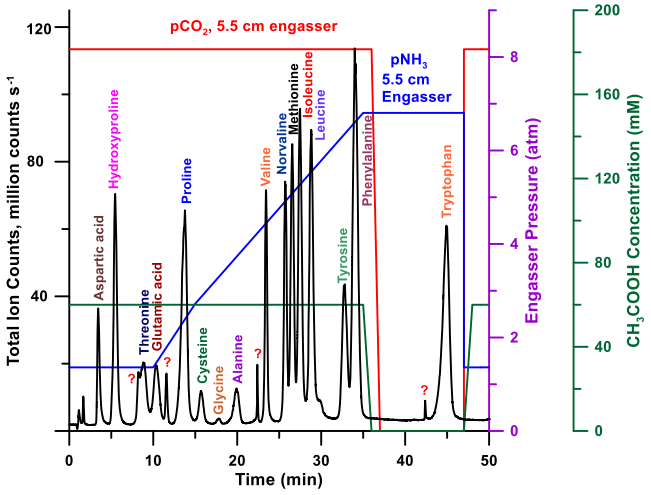

Figure 7. Amino acid (0.1 mM ea.) separation on a short, efficient strong cation exchanger (Hitachi type pH column). The test mixture contained 20 amino acids. Flow rate 0.40 mL/min, 30 °C. Influent (t = 0−35 min 60 mM AcOH).

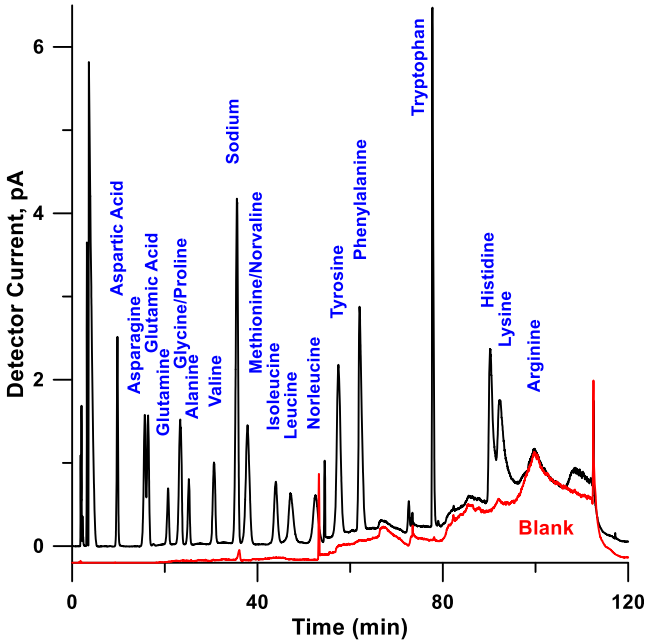

Figure 8. Same conditions as in Figure 6; a charged aerosol detector (CAD) was used. The blank signal was offset by −0.2 pA for clarity.

HCOOH/AcOH cannot easily displace NH_4^+ from strong cation-exchange sites.

The compatibility of the NH_3−CO_2 eluent system with a CAD is shown in Figure 8 for the same amino acid separation. Note that sodium present is detected in this case. The detector background increases in the latter part of the chromatogram as the free NH_3 level going into the detector rises. It is known that large clusters of ammonia molecules can form and may be studied by mass spectrometry after photoionization or electron impact ionization.[36] We surmise that when such clusters pass through a corona discharge, they can acquire a charge to be sensed by the electrometer collection electrode.

Protein Separations Using an NH_3−CO_2 Eluent. We tested the applicability of the same strategy to the separation of five benchmark proteins ranging in MW from 8.6 to 16.9 kDa and in pI from 4.5 to 10.8 using the same cation-exchange mode of separation. We opted to use a column developed for the separation of monoclonal antibodies. This phase utilizes a rigid ethyl(vinylbenzene)-divinylbenzene (55%) nonporous 10 μm support with a superficial sulfonate layer. Figure 9 shows that the proteins generally elute in the order of increasing pI values; separation between the two cytochrome c variants occur in the same order seen in other cation-exchange separations,[37] opposite of what is seen in the reversed-phase mode.[38] To test for adequate buffering, myoglobin retention was studied close to its pI over an injected concentration range of 0.1−10 g/L; no change was noted (Figure S25 and attendant text).

Protein Unfolding, Denaturation, and Supercharging. An unusual aspect of the detailed mass spectra for each of these proteins is the degree of "supercharging." This is illustrated in Figure 10 for myoglobin; compared to the most intense +15 charge state in the benchmark spectrum (red), the most intense peak is the +22 state in the present case (black). Similar supercharging seems to occur in all other cases (Figures S26−S29), albeit for bovine cytochrome, we did not find a suitable benchmark comparison spectrum. There is little doubt that supercharging is caused by unfolding of the protein; the unfolding causes previously inaccessible sites to become available for ion attachment. El-Baba et al.[39] have shown for

https://doi.org/10.1021/acs.analchem.0c05089
Anal. Chem. 2021, 93, 5442−5450

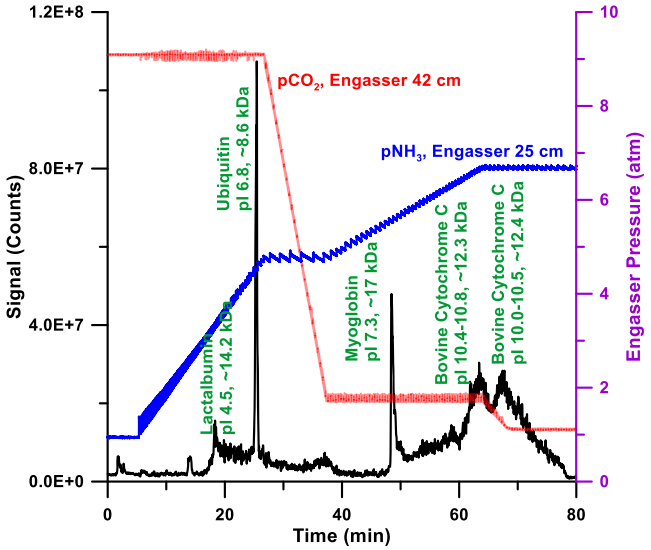

Figure 9. Separation of five proteins on a MAbPac SCX-10 column (2 × 250 mm). Influent 20 mM HCOOH, 0.20 mL/min, and 30 °C.

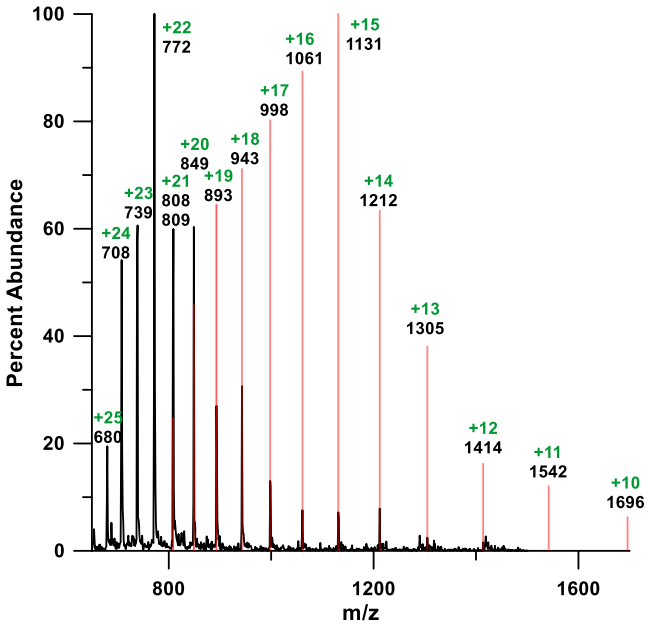

Figure 10. ESI-mass spectra observed for equine myoglobin (taken at t = 48.4 min in Figure 6) in a black trace. Red bars represent digitized relative intensities taken from an illustrative ESI-MS spectrum for the same (taken from http://www.chm.bris.ac.uk/ms/esi-ionisation.xhtml).

ubiquitin how the average charge state increases sigmoidally with increasing temperature, consistent with a two-state, cooperative unfolding transition with a midpoint around the melting temperature of 71 ± 2 °C; in fact, there may be as many as nine stable states involved.

Is supercharging to be avoided or embraced? Cassou et al.[40] argue that it is a boon to MS instruments that have a low m/z ceiling (such as the one used here), enabling the study of proteins and improving MS/MS study of protein ions that have normal native structures and activities in the solutions just prior to electrospray. In contrast, Hedges et al.[29] feel that any process that leads to protein unfolding, and thus supercharging, is to be avoided, especially if protein−protein interactions are to be studied. A potentially useful aspect of the NH_3−CO_2 eluent system is preparative separations as the eluent constituents are volatile. Biologics are the fastest-growing segment in the pharmaceutical industry today. However, preparative separations must utilize conditions where no denaturing occurs, and bioactivity is maintained. This is difficult with organic modifiers. If the present chromatographic conditions led to denaturation, this approach would not be useful. On the other hand, if denaturation/supercharging is caused by the detection (and not the separation) process, this is not a problem. Only a small split stream of the preparative scale effluent needs to be monitored by MS; the unaffected drug material can be recovered in the principal stream.

As to the cause of denaturation, Cassou et al.[40] attribute electrothermal reasons. Hedges et al.[29] provide compelling evidence that in cases where large amounts of gas bubbles out of a solution, the adsorption of proteins, which act like a surfactant, to the gas/liquid interface leads to major conformational changes. In the case of NH_4HCO_3, using myoglobin as a test case, they show convincingly that heat and bubbles act synergistically to cause unfolding during the electrospray process. At room temperature, even in 2 M NH_4HCO_3 (substantially higher ionic strength than present studies), there is no denaturation, a relatively small 7% is denatured on adding HCl to cause minor foaming, ultrasound denatures 14%, and 38% unfolds upon heating (which is accompanied by vigorous foaming). This was not unique to NH_4HCO_3. In 1 M NH_4OAc, ∼99, ∼88, and 88%, respectively, remained unaffected while bubbling N_2, CO_2, or heating alone without gas bubbling, while >98+, and >99+% of the protein denatured on bubbling N_2 and CO_2, respectively, through a heated solution. The preparative scale effluent can be degassed slowly at low temperatures to avoid vigorous bubbling and denaturation.

NH_3−CO_2 Eluent System Allows the Equivalent of Salt Gradients. As its name implies, the column used for the protein separations depicted in Figure 9 was originally developed for the separation and characterization of monoclonal antibodies. This stationary phase is believed to be particularly effective to separate C-terminal lysine variants. The peaks seen in Figure 11 top trace (courtesy Thermo Fisher Scientific) are three different C-terminal lysine variants in a particular commercial monoclonal antibody preparation. Separation of similar variants is an important problem; cation exchange with salt gradient elution is the most commonly recommended.[41] Although an *iso*-pH salt/ionic strength gradient would have been readily possible with a NH_3−CO_2 eluent system, with the help of the vendor, we wished to examine if a pH-gradient elution was possible to affect a similar separation with the high salinity but fully volatile eluent system. Antibody preparations can vary from batch to batch. While the manufacturer provided us with the residual sample used in their chromatogram, even after 10× dilution and moving therefore to a lower monitoring wavelength to gain sensitivity (we lacked a mass spectrometer of high enough mass range to permit MS detection of these antibodies), the available amount allowed for very limited trials. Nevertheless, the lower trace in Figure 11 confirms that a very similar separation is indeed possible. The generally higher background absorbance is likely a consequence of the lower monitoring wavelength.

https://doi.org/10.1021/acs.analchem.0c05089
Anal. Chem. 2021, 93, 5442−5450

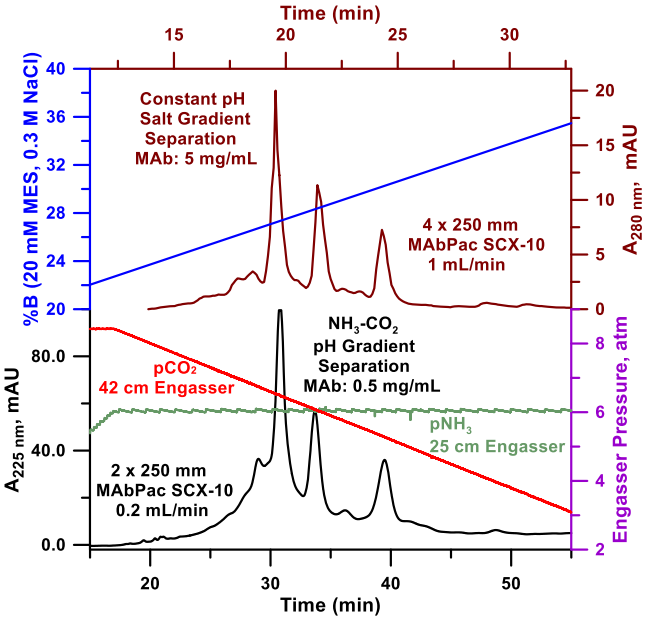

Figure 11. Red-brown trace (top): benchmark separation with a buffered salt gradient eluent system. Both eluents: 20 mM MES, pH 5.6; A and B contain 0.06 and 0.3 M added NaCl, respectively. Elution begins at t = 0 with 15% B. Black trace (bottom) increasing pH-gradient elution using the NH_3−CO_2 system, influent water (see Figure S30 for a more complete picture of the entire chromatogram). A length of 125 μm i.d. tubing at the flow cell exit prevented bubbles, 5 μL injection.

CONCLUSIONS

We present an automated fully volatile eluent preparation system that utilizes high-purity gaseous precursors and can produce eluents across a broad range of salinity. The range of pH attainable with good buffer capacity extends from 4.5 to >10. Although lower pH eluents have been demonstrated with pure CO_2,[15] the addition of a small amount of formic or acetic acid more easily makes a lower pH eluent with good buffering ability.

Ammonium bicarbonate has been previously recognized as a very useful eluent/background electrolyte in HPLC/capillary electrophoresis-ESI-MS/ICP-MS for its complete volatility, good buffering capacity, and the ability to eliminate alkali metal ion adducts.[42,43] In the early days of IC, the merits of a hydroxide eluent for gradient elution were well understood. However, atmospheric CO_2 intrusion continuously changed eluent properties. It was not practical without on-line eluent generation. Users of NH_4HCO_3 know that here, the continuous loss of CO_2 mandates fresh eluent preparation daily. A NH_3−CO_2 based in situ prepared eluent offers much greater versatility in pH and ionic strength variation. Such eluents may also have particular merit in preparative separations of biomolecules. While protein unfolding may occur under electrospray conditions, especially ebullient conditions can be prevented by slow release of pressure in the main effluent stream and cooling the effluent during collection. Despite the merits of automated preparation of completely volatile ionic eluents from high-purity cylinder gases, we recognize that it is a complex system and wide use is unlikely until a commercial version is available.

ASSOCIATED CONTENT

Supporting Information

The Supporting Information is available free of charge at https://pubs.acs.org/doi/10.1021/acs.analchem.0c05089.

Results of computational simulation(XLSX)
Constants used in the numerical simulation, pH contour; surface and buffer intensity plots; engasser arrangement and control schematic; ammonia permeation rate measurement plots; and various mass spectra and total and extracted ion chromatograms (PDF)

AUTHOR INFORMATION

Corresponding Authors

Charles Phillip Shelor − *Department of Chemistry and Biochemistry, University of Texas at Arlington, Arlington, Texas 76019-0065, United States;* orcid.org/0000-0002-2318-9411; Email: Shelor@uta.edu

Purnendu K. Dasgupta − *Department of Chemistry and Biochemistry, University of Texas at Arlington, Arlington, Texas 76019-0065, United States;* orcid.org/0000-0002-8831-7920; Email: dasgupta@uta.edu

Author

Kenji Yoshikawa − *Department of Chemistry and Biochemistry, University of Texas at Arlington, Arlington, Texas 76019-0065, United States*

Complete contact information is available at: https://pubs.acs.org/10.1021/acs.analchem.0c05089

Notes

The authors declare no competing financial interest.

ACKNOWLEDGMENTS

Support from the U.S. National Foundation through grants CHE-1506572 and CHE-2003324 are gratefully acknowledged. We thank Thermo Fisher Scientific and the Hamish Small Chair Endowment at the University of Texas at Arlington for additional support. We thank Hitachi-hta.com and Azypusa.com for the loan of their columns. K.Y. thanks Nihon University for support that enabled his participation.

REFERENCES

(1) Strong, D. L.; Dasgupta, P. K.; Friedman, K.; Stillian, J. R. *Anal. Chem.* **1991**, *63*, 480−486.
(2) Chouhan, B.; Shelor, C. P.; Huang, W.; Chen, Y.; Dasgupta, P. K. *Anal. Chem.* **2020**, *92*, 5561−5568.
(3) Dasgupta, P. K.; Maleki, F. *Talanta* **2019**, *204*, 89−137.
(4) Cui, Y.; Olesik, S. V. *Anal. Chem.* **1991**, *63*, 1812−1819.
(5) Bennett, R.; Olesik, S. V. *Anal. Chim. Acta* **2018**, *999*, 161−168.
(6) Bian, J.; Olesik, S. V. *Analyst* **2019**, *144*, 6270−6275.
(7) Bennett, R.; Biba, M.; Liu, J.; Ahmad, I. A.; Hicks, M. B.; Regalado, E. L. *J. Chromatogr. A* **2019**, *1595*, 190−198.
(8) Décultot, M.; Ledoux, A.; Fournier-Salaün, M.-C.; Estel, L. *J. Chem. Thermodyn.* **2019**, *138*, 67−77.
(9) Gui, X.; Tang, Z.; Fei, W. *J. Chem. Eng. Data* **2011**, *56*, 2420−2429.
(10) National Institutes of Standards and Technology. NIST Chemistry Webbook. SRD69. Carbon Dioxide. Henry's Law Data. https://webbook.nist.gov/cgi/cbook.cgi?ID=C124389&Mask=10#Solubility (accessed Nov 15, 2020).
(11) Stumm, W.; Morgan, J. J. *Aquatic Chemistry*, 2nd ed.; Wiley, New York, 1981; Chapter 4.
(12) Vidal, D. T. R.; Nogueira, T.; Saito, R. M.; do Lago, C. L. *Electrophoresis* **2011**, *32*, 850−856.

(13) Shelor, C. P.; Yoshikawa, K.; Dasgupta, P. K. *Anal. Chem.* **2017**, *89*, 10063−10070.
(14) Shelor, C. P.; Dasgupta, P. K. *J. Chromatogr. A* **2017**, *1523*, 300−308.
(15) Sricharoen, P.; Limchoowong, N.; Shelor, C. P.; Dasgupta, P. K. *Anal. Chem.* **2019**, *91*, 3636−3644.
(16) Gottlieb, A. J.; Crain, D. L. Apparatus and Method for Degassing Liquids. U.S. Patent, US9,114, 3312015.
(17) Gottlieb, A. J.; Kilbridge, W. Apparatus and Method for Degassing Liquids. U.S. Patent, US9,744, 4802017.
(18) Vehovec, T.; Obreza, A. *J. Chromatogr. A* **2010**, *1217*, 1549−1556.
(19) Schilling, K.; Holzgrabe, U. *J. Chromatogr. A* **2020**, *1619*, No. 460911.
(20) Megoulas, N. C.; Koupparis, M. A. *Crit. Rev. Anal. Chem.* **2005**, *35*, 301−316.
(21) Magnusson, L. E.; Risley, D. S.; Koropchak, J. A. *J. Chromatogr. A* **2015**, *1421*, 68−81.
(22) Storm, T.; Reemtsma, T.; Jekel, M. *J. Chromatogr. A* **1999**, *854*, 175−185.
(23) Huber, C. G.; Premstaller, A. *J. Chromatogr. A* **1999**, *849*, 161−173.
(24) Liu, H.; Lam, L.; Chi, B.; Kadjo, A. F.; Dasgupta, P. K. *Anal. Chem.* **2016**, *88*, 2059−2064.
(25) Powell, M. Making LC Methods MS Friendly. October 2013. https://www.agilent.com/cs/library/eseminars/public/Making%20LC%20Methods%20MS%20Friendly.pdf (accessed Nov 16, 2020).
(26) Kunati, S. R.; Yang, S.; William, B. M.; Xu, Y. *J. Pharm. Biomed. Anal.* **2018**, *156*, 189−198.
(27) Wang, Y.; Olesik, S. V. *Anal Chem.* **2019**, *91*, 935−942.
(28) Kenderdine, T.; Xia, Z.; Williams, E. R.; Fabris, D. *Anal. Chem.* **2018**, *90*, 13,541−13,548.
(29) Hedges, J. B.; Vahidi, S.; Yie, X.; Konermann, L. *Anal. Chem.* **2013**, *85*, 6469−6476.
(30) Amornthammarong, N.; Jakmunee, J.; Li, J. Z.; Dasgupta, P. K. *Anal. Chem.* **2006**, *78*, 1890−1896.
(31) Ho, N. S.; Manchester, F. D. *Can. J. Phys.* **1968**, *46*, 1341−1345.
(32) Lim, Y.; Breitbach, Z. S.; Armstrong, D. W.; Berthod, A. *J. Pharm. Anal.* **2016**, *6*, 345−355.
(33) Spackman, D. H.; Stein, W. H.; Moore, S. *Anal. Chem.* **1958**, *30*, 1190−1206.
(34) Hitachi High Technologies Corporation, Tokyo, Japan. Hitachi High-Speed Amino Acid Analyzer L-8900. https://hitachi-hta.com/sites/default/files/literature/L-8900%20Brochure.pdf (accessed Dec 1, 2020).
(35) Hitachi High Technologies America. Amino Acid Analysis of Beer. https://www.hitachi-hightech.com/file/us/pdf/library/application/lc56.pdf (accessed Dec 1, 2020).
(36) Bobbert, C.; Schütte, S.; Steinbach, C.; Buck, U. *Eur. Phys. J. D* **2002**, *19*, 183−192.
(37) Weitzhandler, M.; Farnan, D.; Rohrer, J. S.; Avdalovic, N. *Proteomics* **2001**, *1*, 179−185.
(38) Terabe, S.; Nishi, H.; Ando, T. *J. Chromatogr. A* **1981**, *212*, 295−304.
(39) El-Baba, T. J.; Woodall, D. W.; Raab, S. A.; Fuller, D. R.; Laganowsky, A.; Russell, D. H.; Clemmer, D. E. *J. Am. Chem. Soc.* **2017**, *139*, 6306−6309.
(40) Cassou, C. A.; Sterling, H. J.; Susa, A. C.; Williams, E. R. *Anal. Chem.* **2013**, *85*, 138−146.
(41) Hong, P.; Fountain, K. J.; Wheat, T. E.; Morrison, D. IEX Method Development of a Monoclonal Antibody and Its Charge Variants. Waters Application Note. https://www.waters.com/webassets/cms/library/docs/720003836en.pdf.
(42) Yin, R.; Liu, S.; Zhao, C.; Lu, M.; Tang, M. S.; Wang, H. *Anal. Chem.* **2013**, *85*, 3190−3197.
(43) Dell'mour, M.; Koellensperger, G.; Quirino, J. P.; Haddad, P. R.; Stanetty, C.; Oburger, E.; Puschenreiter, M.; Hann, S. *Electrophoresis* **2010**, *31*, 1201−1207.

https://doi.org/10.1021/acs.analchem.0c05089
Anal. Chem. 2021, 93, 5442−5450